RSC Advances

PAPER

View Article Online
View Journal | View Issue

Cite this: *RSC Adv.*, 2025, **15**, 4607

Enhanced platinum and palladium recovery from aqueous solutions: a comparative study of acylthiourea and amine-modified silica gel adsorbents†

Malehlogonolo R. R. Mphahlele, [a] Alseno K. Mosai,[b] Hlanganani Tutu[a] and Izak A. Kotzé *[a]

The recovery of precious metals from secondary sources is becoming increasingly important due to their natural scarcity and rising industrial demand. This study introduces a novel adsorbent, *N*-triethoxysilylpropyl-*N*′-benzoylthiourea-modified silica gel (TESP-BT-SG), developed for the selective recovery of platinum (Pt) and palladium (Pd) from aqueous solutions that simulate refinery wastewater. The extraction capabilities of TESP-BT-SG were compared with those of an amine-bearing adsorbent, (3-aminopropyl)triethoxy-silane-modified silica gel (APTES-SG), previously recognized for Pt and Pd recovery. Under optimal conditions, TESP-BT-SG achieved extraction efficiencies of 97% for Pt and 99% for Pd. Both adsorbents demonstrated rapid adsorption kinetics for Pd relative to Pt, reaching equilibrium within 3 hours for Pd and within 6 hours (TESP-BT-SG) and 24 hours (APTES-SG) for Pt. In solutions with elevated competing ion concentrations (5–100 mg L^{-1}), both adsorbents retained high selectivity (>97%) for Pt and Pd. Adsorption isotherms and kinetic models were applied to elucidate the adsorption mechanisms, with the Langmuir isotherm and pseudo-second-order models providing the best fits, indicating monolayer coverage and chemisorption, respectively. Notably, the APTES-SG sorbent demonstrated enhanced performance with an increased loading capacity of 2.45 mmol g^{-1} compared to the previously reported 1.15 mmol g^{-1}, achieved through our improved synthesis method. This modified APTES-SG showed significantly higher affinity for Pd (98%), Pt (97%), and iridium (Ir) (89%) compared to previous values of 8%, 33%, and 42%, respectively. The exceptional efficiency and selectivity of these silica-anchored adsorbents underscore their potential as cost-effective solutions for industries seeking to recover precious metals.

Received 7th November 2024
Accepted 29th January 2025

DOI: 10.1039/d4ra07935c

rsc.li/rsc-advances

1. Introduction

Platinum group metals (PGMs), particularly platinum (Pt) and palladium (Pd), are essential components in various industries, including catalytic converters, electronics, pharmaceuticals, and, more recently, the hydrogen fuel cell sector.[1–3] These diverse applications arise from their unique properties, such as corrosion resistance, high melting points, and remarkable catalytic activities.[1–3] Despite their high cost, demand for PGMs continues to grow due to their irreplaceable roles in key industrial processes.[4] Combined with their low natural abundance in the Earth's crust (0.0063 ppm), the rising demand may lead to potential shortages.[3,4] Consequently, there is growing interest in exploring the recovery of these metals from secondary sources, such as refinery holding ponds and industrial waste, which may contain recoverable amounts of Pt and Pd (27–120 mg kg^{-1}).[2–5] In addition to PGMs, metals such as magnesium, nickel, manganese, copper, calcium, and iron (Mg, Ni, Mn, Cu, Ca, and Fe) can also enter the environment through industrial wastewater.[6,7] Prolonged exposure and accumulation of these metals in the environment can lead to detrimental effects on mammals, plants, and humans.[6–8] Recovering these metals from secondary sources with efficient separation techniques is thus both economically and environmentally advantageous.[6,7]

Conventional recovery techniques used for removing PGMs from aqueous solutions include chemical precipitation, solvent extraction, and ion exchange.[2,8,9] However, these methods often suffer from low efficiency, poor selectivity, and the generation of secondary waste.[4,6,9] To overcome these limitations, there has been a growing focus on developing alternative methods, such as adsorption, which offer higher efficiency, selectivity, and ease

[a]*Molecular Sciences Institute, School of Chemistry, University of the Witwatersrand, Private Bag X3, WITS, Johannesburg, 2050, South Africa. E-mail: Izak.Kotze@wits.ac.za*

[b]*Department of Chemistry, Faculty of Natural and Agricultural Sciences, University of Pretoria, Lynnwood Road, Pretoria 0002, South Africa*

† Electronic supplementary information (ESI) available. See DOI: https://doi.org/10.1039/d4ra07935c

of operation.[4,8,9] Adsorption utilises solid supports, such as activated carbon, membranes, polymer resins, mesoporous silica, zeolite, and graphene oxide.[4] These supports can be tailored to improve selectivity towards target ions, thus enhancing overall efficiency.[4]

In PGM separation studies, selectivity is a crucial parameter, as these metals are typically found alongside other transition metals.[9–12] Adsorption has proven superior to traditional separation techniques, which are limited in their ability to selectively recover individual PGMs without co-extracting other ions.[11–14] PGM-targeted adsorbents typically contain nitrogen (N), oxygen (O), and sulphur (S) bearing ligands.[4,9,11] According to the hard–soft acid–base (HSAB) theory, Pt and Pd are classified as soft metals, thus having a high affinity for soft bases (S > N > O).[4,15,16] Therefore, using ligands that contain soft donor atoms can be advantageous for the selective recovery of Pt and Pd from solutions containing a wide array of metal ions.[4,13–16]

In our previous work, we developed a novel acylthiourea-modified silica gel adsorbent, *N*,*N*-di(trimethoxysilylpropyl)-*N*′-benzoylthiourea-modified silica gel (DTMSP-BT-SG) (Fig. 1a), for recovering Pt and Pd from aqueous solutions.[17] The acylthiourea ligand class was chosen for its multiple advantages, including:

(1) Absence of toxicity, sensitivity, and odour,
(2) Facile two-step one-pot synthesis,
(3) Multiple donor atoms (N, O, S), and
(4) High affinity for PGMs.[10,17]

We demonstrated the simplicity of synthesising this ligand (74% yield) and its successful immobilisation onto silica gel.[17] The DTMSP-BT-SG adsorbent achieved Pt and Pd removal efficiencies of >98%, with adsorption capacities of 48.52 mg g^{-1} (Pt) and 29.68 mg g^{-1} (Pd).[17] Moreover, the adsorbent maintained enhanced selectivity for Pt and Pd (>80%) even in the presence of high concentrations of competing ions. It also outperformed a silica-anchored amine adsorbent, bis(3-(trimethoxysilyl)propyl)amine-modified silica gel (BTMSPA-SG) (Fig. 1b), which was also used in the recovery studies.[17] These findings established silica-anchored acylthioureas as promising adsorbents for Pt and Pd recovery from refinery wastewater.

Herein, we expand upon our previous work by exploring the synthesis of a second silica-anchored acylthiourea adsorbent (TESP-BT-SG, Fig. 1c) featuring one pendent chain to immobilise the ligand onto the solid support. This design aims to make the nitrogen donor atom more accessible by reducing steric hindrance. Additionally, we significantly enhanced the synthesis of another amine variant (APTES-SG, Fig. 1d) for Pt and Pd recovery from aqueous solutions (Schemes S1 and S2†). Our modified methodology achieved a ligand loading of 2.45 mmol g^{-1} on the solid support, compared to the previously reported value of 1.15 mmol g^{-1}.[11,12] Several parameters, including dosage, pH, concentration, and competing ions, were varied to simulate refinery wastewaters. Furthermore, pK_a studies and extensive characterisation were conducted to gain insights into the properties of the adsorbents and their relationship to extraction efficiencies.

These findings establish silica-anchored acylthioureas as promising adsorbents for the recovery of Pt and Pd from refinery wastewater.

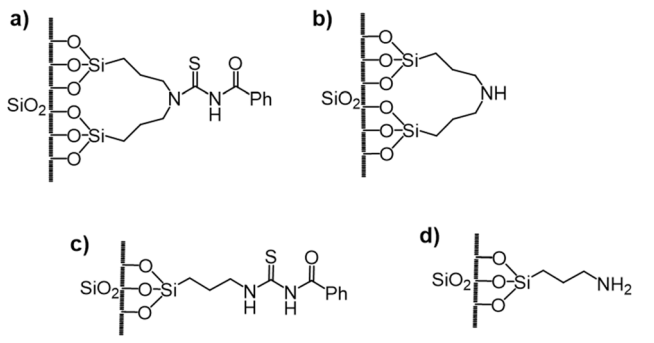

Fig. 1 Adsorbents used: (a) DTMSP-BT-SG, (b) BTMSPA-SG, (c) TESP-BT-SG and (d) APTES-SG.

2. Materials and methods

2.1. Reagents

The synthetic reagents (benzoyl chloride, potassium thiocyanate (KSCN), and (3-aminopropyl)triethoxysilane (APTES)) and analytical grade standards (platinum (Pt) and palladium (Pd) standard solutions (1000 mg L^{-1} in 5% w/w of *c*(HCl))) were purchased from Sigma Aldrich, South Africa, and used without further purification. To prepare the stock solutions, the Pt and Pd standard solutions (1000 mg L^{-1} in 5% w/w of *c*(HCl)) were diluted with deionised water to obtain the desired concentrations. The solutions were preserved by adding drops of HCl and stored in the refrigerator at 4 °C. To obtain the desired pH of the solutions, 0.01 mol L^{-1} of HCl and NaOH were used together with a pH meter (Mettler Toledo, Switzerland).

2.2. Characterization techniques

The one- and two-dimensional nuclear magnetic resonance (NMR) spectra were obtained using a Bruker Avance III 500 MHz (Germany) to confirm the molecular structure of the ligand. Mass spectrometry was performed using a high-resolution Bruker Compact Q-TOF spectrometer (Germany) to determine the mass-to-charge ratio (*m*/*z*) of the ligand. The functional groups of the ligand and adsorbents were determined using Fourier transform infrared spectroscopy (FT-IR) (Tensor 27, Bruker, Germany). Scanning electron microscopy (SEM) (TESCAN Vega, Czech Republic) was used to observe the surface morphology of the adsorbents. X-ray fluorescence (XRF) (PAnalytical, Netherlands) and powder X-ray diffraction (PXRD) (D2 Phaser, Bruker, Germany) were used to study the chemical compositions and mineralogy of the adsorbents, respectively. The surface area and pore characteristics were determined with Brunauer–Emmet–Teller (BET) N_2 adsorption–desorption isotherms (TriStar 3000 V6.05 A, Micrometrics, USA). The thermal stability of the adsorbents was assessed using thermogravimetric analysis (TGA) and differential thermal analysis (DTA) (PerkinElmer Pyris 1 TGA, Massachusetts, USA). Elemental analysis was carried out using varioELcube V4.0.13, Elementar (Germany) for determination of the C, H, N, and S elemental compositions present on the silica gel. Inductively coupled plasma optical emission spectroscopy

(ICP-OES) (Spectro Genesis, Germany) was used to determine the concentrations of the metal ions.

2.3. Synthesis of *N*-triethoxysilylpropyl-*N*′-benzoylthiourea (TESP-BT)

The synthesis of TESP-BT (Scheme S1, ESI†) was carried out by first dissolving potassium thiocyanate (1.0 g/10 mmol) in anhydrous acetonitrile (20 mL).[10,17] Benzoyl chloride (1.2 mL/10 mmol) in acetonitrile (15 mL) was added dropwise to the solution and it was heated under reflux for 1 h. The reaction mixture was cooled to room temperature and then placed under reduced pressure for 2 h to remove the acetonitrile. To the remaining residue, anhydrous dichloromethane (DCM) (20 mL) was added, followed by a dropwise addition of (3-aminopropyl) triethoxysilane (APTES) (2.2 mL/9.5 mmol) in DCM (20 mL). The mixture was left to stir overnight at 40 °C to yield the product as a yellow liquid containing white particles. The reaction mixture was filtered, and the filtrate was placed under reduced pressure to remove the solvent. A yellow oil was obtained as the final product. A yield of 79% was obtained and the product was characterized by NMR and FT-IR spectroscopy, as well as mass spectrometry. ^{1}H NMR (500 MHz, $CDCl_3$), δ(ppm): 10.74 (s, 1H: N–H), 9.10 (s, 1H: N–H), 7.78–7.80 (d, J = 8.0, 8.0 Hz, 2H, H^h, H^l), 7.57 (t, J = 8 Hz, 1H, H^j), 7.45 (t, J = 8.0, 8.0 Hz, 2H, H^i, H^k), 3.79 (q, J = 6.67 Hz, 6H, H^b), 3.66 (q, J = 6.67 Hz, 2H, H^e), 1.80 (t, J = 8.0 Hz, 2H, H^d), 1.20 (t, J = 8.0 Hz, 9H, H^a), 0.67 (t, J = 8.0 Hz, 2H, H^c). ^{13}C NMR (400 MHz) ($CDCl_3$), δ (ppm): 179.39 (C═S), 166.57 (C═O), 133.07 (C^9), 131.49 (C^6) 128.67 (C^8, C^{10}), 127.13 (C^7, C^{11}), 55.09 (C^2), 47.86 (C^5), 21.44 (C^4), 17.94 (C^1), 7.44 (C^3). FT-IR: ν (cm^{-1}): 3246 (N–H), 2974, 2928, 2886 (C–H), 1671 (C═O), 1080 (Si–O–Si). Chemical formula: $C_{17}H_{28}N_2O_4SSi$, ESI-MS (m/z): calc. 385.15 [M], exp. 385.1 $[M + H]^+$.

2.4. Immobilization of TESP-BT and APTES onto silica gel

The procedure (Scheme S2†) reported by Erdem *et al.*, was used to immobilize TESP-BT and APTES onto the silica gel (Davisil Grade 710, pore size 50–76 Å).[18,19] This method involved pre-activation of the silica gel (0.50 g) by first stirring it in 0.01 M acetic acid (20 mL) for 10 min. The activated silica was filtered on a suction pump and washed several times with deionized water. The silica gel was added to a flask containing toluene (20 mL) and TESP-BT (0.30 mL), and thereafter stirred under reflux (110 °C) for 20 h. The reaction mixture was cooled to room temperature, filtered, and washed with toluene. The obtained functionalised silica particles were left to dry in the oven at 80 °C for 8 h. The immobilisation of APTES onto the silica gel was carried out in a similar manner (Scheme S2b†).

2.5. Batch adsorption studies

The adsorption experiments (Fig. S1†) were conducted by pre-weighing the required mass of adsorbent into 50 mL centrifuge tubes, along with 20 mL of the relevant metal standard solution. The tubes were placed on an elliptical benchtop shaker to agitate at 150 rpm at room temperature. After mixing, the samples were centrifuged at 30 rpm for 5 min, to separate the metal-loaded adsorbent from the liquid. Subsequently, the samples were filtered, and the metal concentrations of the filtrates were measured using ICP-OES. The effects of adsorbent dosage (5–50 mg), pH (2–9), initial concentration (0.5–50 mg L^{-1}), contact time (0–1440 min), and competing ions (Rh, Ir, Ru, Fe, Ca, Mg, K, Co, Ni, Zn) were studied. These parameters were investigated to simulate conditions of refinery wastewater and to determine the optimal conditions for the adsorption of Pt and Pd by TESP-BT-SG and APTES-SG. The adsorption capacity, q_e (mg g^{-1}) and adsorption efficiency (%) were calculated using equations eqn (1) and (2) respectively.

$$q_e = \left(\frac{(C_0 - C_e)V}{m}\right) \quad (1)$$

$$\text{Adsorption efficiency} = \frac{(C_0 - C_e)}{C_0} \times 100\% \quad (2)$$

where C_0 and C_e (mg L^{-1}) denote the initial and equilibrium metal concentrations respectively. V (mL) is the solution volume and, m (g) is the mass of the adsorbent used.[2,4]

2.6. pK_a determination experiments

To determine the pK_a's of the adsorbents, titration experiments were performed with a potentiometric titrator (Metrohm, Switzerland), and a pH meter. The experiments were carried out by adding 50 mg of adsorbent and 40 mL of deionized water into a beaker. The contents were stirred until the pH of the solution stabilized, and the initial pH of the adsorbent was recorded. To titrate the solutions, 0.01 M HCl and NaOH were used to titrate the bases and acids respectively. pH values and volumes of titrant added were recorded until the endpoints were reached. The obtained readings were used to plot a curve of pH *versus* volume. To determine the pK_a's, the Henderson–Hasselbach equation eqn (3) was used, and the alternative basic equation eqn (4) was used to determine the pK_b's.[20–26]

$$\text{pH} = \text{p}K_a + \log\frac{[A^-]}{[HA]} \quad (3)$$

$$\text{pOH} = \text{p}K_b + \log\frac{[BH^+]}{[B]} \quad (4)$$

2.7. Statistical analysis

All the experiments were conducted in duplicate ($n = 2$), and the mean values were used for data analysis. Data processing was performed using Microsoft Excel. The relative standard deviation (RSD) and relative standard error (RSE) of the measurements were calculated, with RSD values below 4% and RSE values below 3%.

3. Results and discussion

3.1. Characterization of *N*-triethoxysilylpropyl-*N*′-benzoylthiourea (TESP-BT)

The molecular structure of TESP-BT was confirmed by one- and two-dimensional NMR spectroscopy, FT-IR spectroscopy, and

mass spectrometry. The ^{1}H NMR spectrum (Fig. S2†) displayed two singlets at 10.74 and 9.10 ppm corresponding to the amidic protons (NH^{f} and NH^{g}). H^{f} coupled to the quartet (H^{e}) at 3.66 ppm on COSY (Fig. S3†) thus, distinguishing it from H^{g}. In the aromatic region (7.45–7.80 ppm), the deshielded doublet at 7.80 ppm was assigned to H^{h} and H^{l}, which both experience the electron-withdrawing effect of the carbonyl substituent. The COSY spectrum was used to assign H^{i}/H^{k} and H^{j} at 7.45 and 7.57 ppm respectively. In the aliphatic region, H^{b} (3.79 ppm) and H^{e} (3.66 ppm) were found to be the most deshielded due to the adjacent electronegative oxygen and nitrogen atoms respectively. H^{d}, H^{a} and H^{c} were found upfield from 1.80–0.67 ppm.

In the ^{13}C NMR spectrum (Fig. S4†), the carbonyl (C=O) and thiocarbonyl (C=S) carbons were assigned to the deshielded signals at 179.39 and 166.57 ppm respectively. HMBC (Fig. S5†), revealed that C=S coupled to H^{e} through long-range coupling hence it was distinguished from C=O. The assignment of the aromatic (C^{7}, C^{8}, C^{9}, C^{10}, C^{11}) and aliphatic carbons (C^{5}, C^{4}, C^{3}, C^{2}, C^{1}) were achieved with HSQC (Fig. S6†) for C–H correlation, together with ^{13}C DEPT (Fig. S7†). The signal at 131.49 ppm corresponding to a quaternary carbon was assigned to C^{6}.

TESP-BT was further characterized by FT-IR spectroscopy (Fig. S8†), which indicated the weak N–H stretch at 3246 cm^{-1}. The C=O stretch was found at 1671 cm^{-1} whilst the C=S stretch can be assumed to be in the regions 800–1500 cm^{-1}, which is characteristic of acylthioureas.[10,27,28] The strong Si–O–Si stretch at 1080 cm^{-1} further confirmed the ligand structure.

Mass spectrometry (Fig. S9†) also confirmed the identity of TESP-BT as the predicted isotopologue pattern agreed with the experimentally obtained spectrum. The ESI-MS $[M + H]^{+}$ of 385.15 *m*/*z* was observed and it correlated with the calculated mass of 385.15 *m*/*z*.

3.2. Characterization of the adsorbents

The FT-IR spectra of the silica gel, TESP-BT ligand, and TESP-BT-SG adsorbent are illustrated in Fig. 2a. The silica gel is usually characterized by strong bands which are found in the low-frequency region (1000–500 cm^{-1}).[29,30]

These bands correspond to the Si–O–Si asymmetric and Si–O symmetric stretches at 1085 and 490 cm^{-1} respectively.[29,30] The additional silica bands observed at 1649, and 3500 cm^{-1} are usually attributed to the bending vibrations of physically adsorbed H_2O molecules and OH vibrations respectively and these are caused by the hydrogen-bonded surface silanol groups.[29–31]

Upon functionalization of TESP-BT onto the silica gel, there was an appearance of new peaks at 3245, 2900 and 1688 cm^{-1}, which are respectively due to the N–H, C–H and C=O groups. For the APTES-SG adsorbent (Fig S10†), two bands were observed at 3200 and 2928, and 2582 cm^{-1} which corresponded to the NH and CH_2 groups of APTES, thus confirming that the desired adsorbent was obtained.[29]

^{13}C Solid-state NMR (Fig. 2b) further confirmed the functionalization of TESP-BT and APTES onto the silica gel. The aliphatic CH_2 carbons (C_3, C_4 and C_5) of both APTES-SG and

TESP-BT-SG were assigned to the peaks at 8.4, 16.5, and 43.2 ppm respectively. In the aromatic region of TESP-BT-SG, additional peaks were observed at 121.8, 161.2 and 174.9 ppm and these respectively corresponded to the aromatic, C=O and C=S carbons of the TESP-BT ligand. Interestingly, these peaks were significantly sharper than the C=O and C=S signals observed for the DTMSP-BT-SG reported previously.[17]

The PXRD patterns (Fig. 3a) of the adsorbents were all characterized by a dominant peak at $2\theta = 21.9°$, which is known to be indicative of the amorphous nature of the materials.[31,32] The BET N_2 isotherms (Fig. 3b) obtained are classified as type IV isotherms, which denote adsorption taking place in two stages.[33,34] The initial stage involves filling of the micropores, whilst the second stage is due to filling of the mesopores.[33,34] Fig. 3b also indicates that after the immobilization process, there was a reduction in the amount of N_2 adsorbed, which is evidence that both TESP-BT and APTES were incorporated into the silica gel and as a result blocked access of more N_2 gas molecules.[29,34] Furthermore, the decrease in surface area and pore volumes (Table S1†) after the ligand immobilization proves that the silica surface and channels were covered and filled with the functional groups.[29,34]

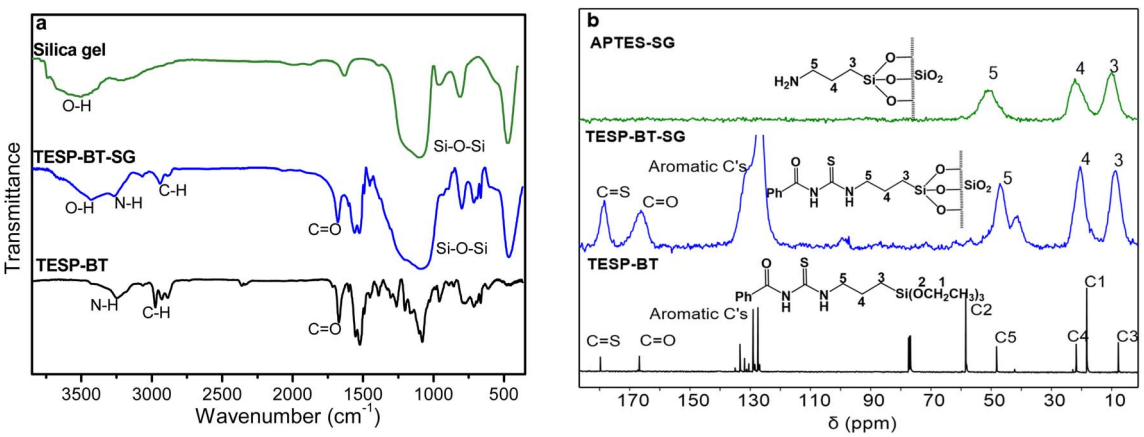

Fig. 2 The (a) FT-IR and (b) ^{13}C NMR spectra of the adsorbents.

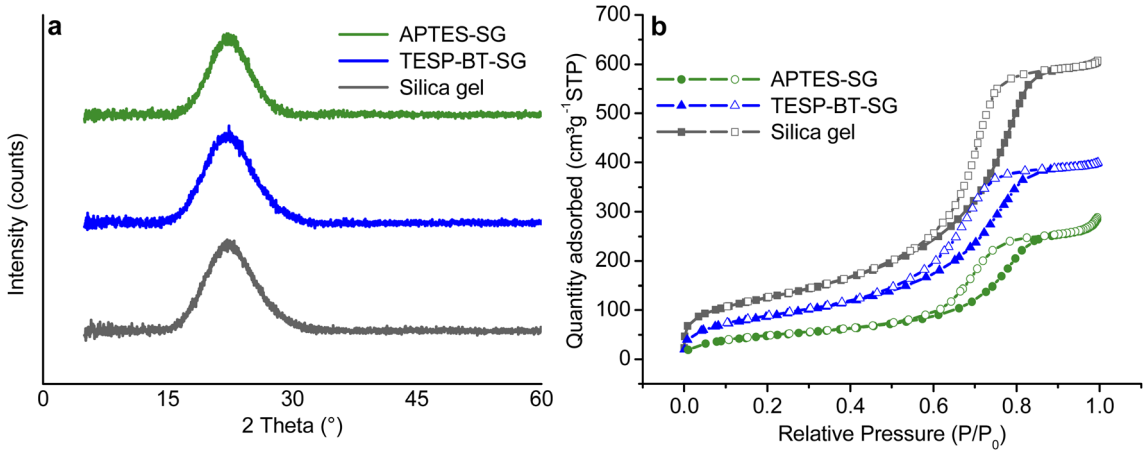

Fig. 3 (a) PXRD patterns and (b) BET N_2 adsorption (●) desorption (○) isotherms of the adsorbents.

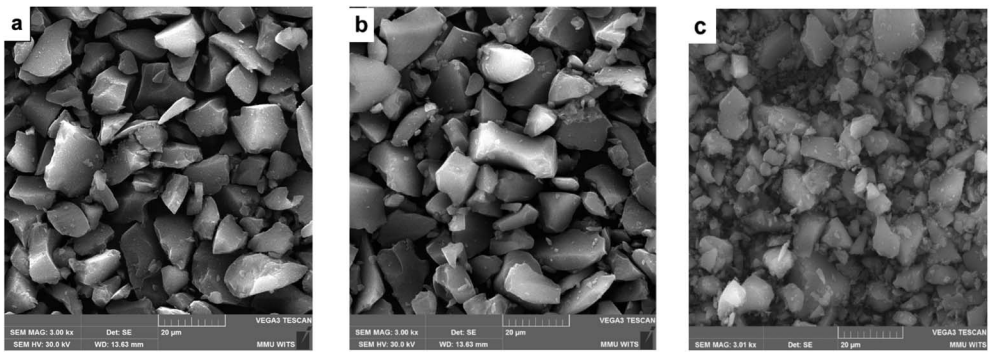

Fig. 4 SEM images of (a) silica gel and (b) TESP-BT-SG and (c) APTES-SG.

The SEM images (Fig. 4) indicated that all the adsorbents exhibited a non-uniform surface containing particles of various sizes and shapes.[32] The reduction in particle size observed in Fig. 4c can be attributed to mechanical abrasion which occurs during stirring in the adsorbent synthesis.[33]

The oxide chemical compositions of the adsorbents were determined by XRF (Table S2†). The unmodified silica gel was dominantly composed of an SiO_2 content of 89.2%, which decreased to 78.81% (TESP-BT-SG) and 79.41% (APTES-SG), after the immobilization process. Perez *et al.* reported that the lower SiO_2 content observed for TESP-BT-SG and APTES-SG indicates that the acylthiourea and amine groups are bound to the silica gel.[29]

Table 1 lists the elemental compositions of the unmodified silica gel and the adsorbents. The increased content of C, H, N and S after the immobilization process, further confirmed the introduction of the functional groups onto the silica gel to form TESP-BT-SG and APTES-SG.[29,34] Additionally, the reported C and N elemental compositions of the adsorbents were used to calculate the ligand concentrations, which aided in calculating the theoretical loading capacities of the adsorbents in the extraction experiments.

Table 1 Elemental analysis of the adsorbents

	C		H	N		S
Adsorbents	%	mmol g^{-1}	%	%	mmol g^{-1}	%
Silica gel	0.0		0.86	0.0		0.0
TESP-BT-SG	8.32	0.630	1.26	1.55	0.553	1.26
APTES-SG	9.84	2.731	2.44	3.43	2.448	0.0

The thermal stability of the adsorbents was also determined and the TGA and DTA graphs of the silica gel, TESP-BT-SG and APTES-SG are presented in Fig. S11.† There was a two-stage weight loss trend observed on the graphs.[30,31,35] The first stage between 25–100 °C, measured a 2–5% weight loss which is due to dehydration of adsorbed water molecules from adsorbents.[30,31,35,36] In the second stage (100–800 °C), a further 4% weight loss was observed for the silica gel and a 15–18% loss was recorded for TESP-BT-SG and APTES-SG. The high quantity of weight loss observed for TESP-BT-SG and APTES-SG relative to the silica gel has been reported to be due to the loss of the functional groups anchored from the silica surface.[35,36]

The determined pK_a and pK_b plots of the adsorbents are tabulated below (Table 2), and the plots are reported in the ESI (Fig. S12†). The initial pH results of the adsorbents indicated that the acylthioureas were weak acids (pH 3–4), whilst the amines were weak bases (pH 6–8), hence the solutions were

Table 2 Determined pK_a and pK_b values of adsorbents

Acylthiourea adsorbents	pK_a	Amine adsorbents	pK_b
DTMSP-BT-SG	5.65	BTMSPA-SG	11.84
TESP-BT-SG	5.87	APTES-SG	11.92

titrated with strong base (NaOH) and strong acid (HCl) respectively. When determining the pK_a of weak acids, the volume added at half the equivalence point is considered because half-neutralization occurs here and the concentrations of the weak acid and conjugate base are at this point, hence the Hasselbalch equation eqn (3), becomes pH = pK_a (Fig. S12a and b†).[18–23] Similarly, when determining the pK_b of weak bases, the midpoint which is located halfway between the initial point and equivalence point is considered (Fig. S12c and d†). At the midpoint, the number of moles of strong acid added, is equal to half the number of moles of the base that were initially in the flask. Thus, at the midpoint, the basic form of Henderson–Hasselbalch equation eqn (4) becomes pOH = pK_b.[18,21–26]

3.3. Adsorption studies

3.3.1. Effect of mass. The effect of mass (5–50 mg) (Fig. 5a) on Pt and Pd removal by TESP-BT-SG and APTES-SG indicated that the adsorption efficiency increased with adsorbent mass. This was expected, as a higher dosage increases the number of active sites thus, more Pt and Pd were captured.[13,14,37] TESP-BT-SG recovered >97% Pt and Pd at all the studied dosages. APTES-SG also recovered >97% Pd (5–50 mg), however, Pt removal was observed to be the lowest (<83%) at 5 mg.

Compared to our previous results, the silica-anchored acylthioureas (TESP-BT-SG and DTMSP-BT-SG) displayed similar trends of Pt and Pd recovery, which can be attributed to the similarity in their active sites.[17] The obtained maximum experimental adsorption capacities (q_{max}) and calculated adsorbent-to-metal ratios (Table S3†) of both adsorbents were also quite comparable, thus validating the similarity in their Pt and Pd extraction efficiencies. An increase in Pt and Pd adsorption was observed for the current silica-anchored amine (APTES-SG), whilst previously BTMSPA-SG recorded a low Pt (40%) and Pd (90%) uptake.[17] The enhanced recovery displayed by APTES-SG can be attributed to its higher ligand concentration (2.448 mmol g^{-1}) and superior adsorption capacities (25.06 mg g^{-1} (Pt) and 32.73 mg g^{-1} (Pd)) that surpassed those of BTMSPA-SG, which had a ligand concentration of 1.68 mmol g^{-1} and adsorption capacities of 6.63 mg g^{-1} (Pt) and 12.53 mg g^{-1} (Pd)).[14,15,17,38]

Nikoloski *et al.*, reported that the active sites formed by the surface functional groups of the adsorbents are among one of the most dominant factors that can influence the extent of adsorption, alongside the solution's acidity and the presence of competing ions.[15,38] Thus, the presence of one donor atom (N) on the amines *versus* three atoms (S, N, O) on the acylthioureas, accounts for their superiority in adsorption. From the results above, it can also be confirmed that the high adsorption exhibited by APTES-SG over BTMSPA-SG is a result of its elevated ligand concentration, which offers more active sites to capture the metals. The optimum dosage of adsorption was 0.5 and 2.5 g L^{-1} for Pd and Pt respectively, for both adsorbents.

3.3.2. Effect of pH on the uptake of Pt and Pd. Studies have indicated that the pH of solutions can strongly influence the adsorption behaviour and efficiency, hence, the role of pH (2–9) (Fig. 5b) was studied.[37–39] The highest Pt and Pd (>82.5%) removal by TESP-BT-SG and APTES-SG was observed at pH 2.

This occurs because the concentration of hydronium ions (H^+) is high at very low pH values and therefore, act to protonate the adsorbent surface functional groups.[39] The primary amine group of APTES-SG will form NH_3^+ upon protonation.[39] Whilst for TESP-BT-SG, a kinetic study done by Congdon and Edward, indicated that the sulphur atom of the *N*′-benzoylthiourea group gets protonated first, followed by a second protonation of the amidic moiety with increasing acid concentration.[28,40] The protonation of these groups will contribute to positively charged adsorbents' surfaces, thus inducing adsorption through the ion-pairing mechanism where the most dominant and stable Pt and Pd chloro-complexes ($[PtCl_6]^{2-}$ and $[PdCl_4]^{2-}$) will get captured.[39,41,42] Many studies have reported that whilst the ion-pairing mechanism is more pronounced in the acidic regions, adsorption is not exclusive to only electrostatic attractions, but

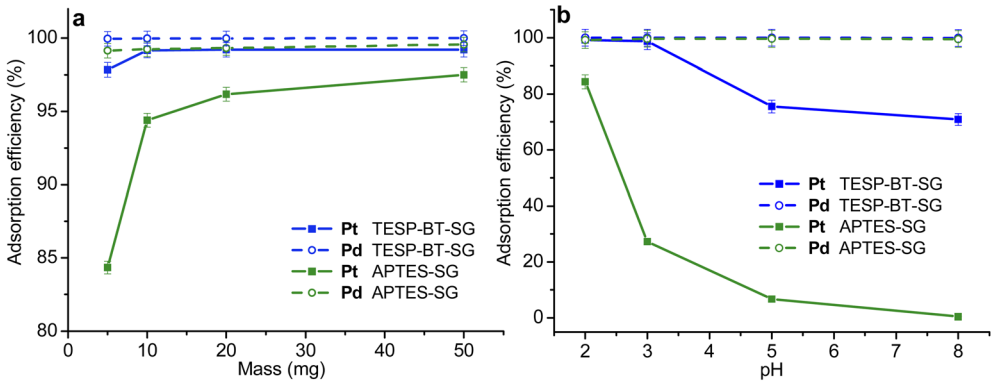

Fig. 5 Effect of (a) mass and (b) pH on the recovery of Pt and Pd (mass = 10 mg, pH = 2, conc. = 5 mg L^{-1}, time = 4 h, temp. = 25 °C, vol. = 20 mL, n = 2, RSD < 4%).

it can simultaneously take place with other mechanisms including ion exchange, chelation, and metal reduction.[42–45]

At pH > 2, the Pt removal efficiency decreased, especially for APTES-SG, whilst for Pd, adsorption remained high at these conditions. The adsorption of Pt and Pd has been reported to decrease at higher pH regions due to the low concentration of Cl^- ions that normally form the stable chloro-complexes and as a result, hydrolysis occurs, forming aqua species which are known to be less adsorbable.[44,45] Chassary *et al.*, reported that Pt(IV) is more sensitive to hydrolysis relative to Pd(II), thus it readily forms these diverse aqua species ($[PtCl_5(H_2O)]^-$ and $[PtCl_4(H_2O)_2]$) which aren't prone to adsorption, hence the observed decrease in Pt recovery.[42] The high Pd recovery indicates that the present Pd(II) aqua species ($[PdCl_2(H_2O)_2]$, $[PdCl_3(OH)]^{2-}$, $[PdCl(OH)_3]^{2-}$) are still favourable for adsorption by both adsorbents.[11,46] The difference in the adsorbents' efficiencies towards the two metals has also frequently been attributed to the varying ionic radius of their anionic complexes ($[PdCl_4]^{2-}$ and $[PtCl_6]^{2-}$), as functional groups on the adsorbent surfaces will tend to approach the Pd complexes, which have a smaller radius.[42,43]

Additionally, the lack of hydronium ions in these basic regions, means that the dominant mechanism of adsorption will likely be through chelation of the metals to the acylthiourea, and amine groups of the adsorbents.[39,41,42]

The Pd adsorption behaviour by TESP-BT-SG was fairly similar to DTMSP-BT-SG in our previous work however, for Pt, the recovery decreased in the basic regions, as previously a >98% efficiency was observed at pH 8, whilst currently it dropped to 77%.[17] For the silica-anchored amines, APTES-SG currently performed better than the previous BTMSPA-SG adsorbent in the Pd adsorption as a low recovery of 70% was observed for the latter, whilst presently its >97%.[17] The Pt recovery efficiencies by both the silica-anchored amines were comparable.[17] The pH results proved both acylthioureas (TESP-BT-SG and DTMSP-BT-SG) to be better adsorbents than the amines (BTMSPA-SG and APTES-SG) as they sustained great adsorption capability in the acidic and basic regions.

3.3.3. Effect of Pt and Pd concentration. The study on the effect of Pt and Pd concentration (2–50 mg L^{-1}) showed that Pd removal by TESP-BT-SG and APTES-SG decreased as concentrations exceeded 2 mg L^{-1} (Fig. 6a). For Pt, an initial increase in uptake was observed between 2–10 mg L^{-1} for both adsorbents, likely due to the high availability of active sites at lower metal concentrations.[13,14] Beyond 10 mg L^{-1}, the removal efficiency declined, suggesting that the active sites on the adsorbents were becoming saturated as more metals were captured at higher concentrations. As a result, adsorption could no longer proceed beyond this point.

An improvement in adsorption was noted for APTES-SG, which achieved maximum Pt and Pd recoveries of 91% and 98%, respectively, compared to the previously reported BTMSPA-SG with maximum adsorptions of 45% (Pt) and 94% (Pd). The silica-anchored acylthioureas recorded similar removal efficiencies under these conditions. Optimal Pt and Pd concentrations for adsorption were observed at 5 mg L^{-1} for TESP-BT-SG. For APTES-SG, the optimal concentration was 5 mg L^{-1} for Pd and 10 mg L^{-1} for Pt.

3.4 Adsorption isotherms

The Langmuir, Freundlich, and Dubinin–Radushkevich (D–R) isotherms are among the most generally used models to describe the equilibrium adsorption relationship between the absorbents and the metals.[15,38,39] The Langmuir isotherm model (eqn (5)) describes the adsorption sites on the adsorbent as structurally homogenous, and energetically equivalent.[6,39] This model also assumes a finite number of sites or capacity on the adsorbent, therefore if no further adsorption takes place, then the saturation value has been reached.[6,39] Moreover, the Langmuir model describes adsorption to take place in a monolayer fashion.[6]

$$\frac{C_e}{q_e} = \left(\frac{1}{q_m}\right) C_e + \left(\frac{1}{K_L q_m}\right) \quad (5)$$

q_m (mg g^{-1}) is the maximum amount of metal adsorbed on the adsorbent for complete monolayer coverage.[15,38,39] K_L (L mol^{-1})

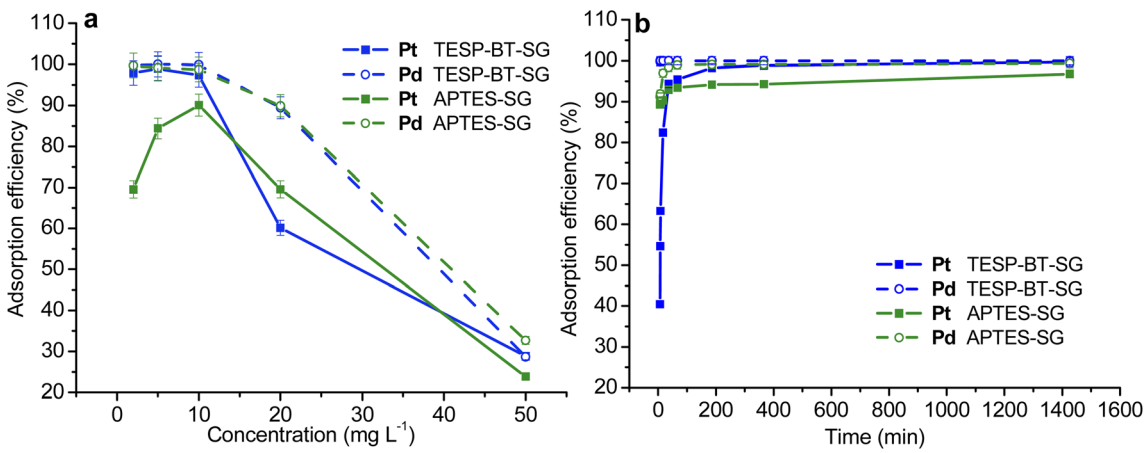

Fig. 6 Effect of (a) concentration (b) contact time on the recovery of Pt and Pd (mass = 10 mg, pH = 2, time = 4 h, conc. = 5 mg L^{-1}, temp. = 25 °C, vol. = 20 mL, n = 2, RSD < 4%).

is the Langmuir isotherm constant that is related to the affinity of the binding sites and indicates the adsorption selectivity of the adsorbent for a particular metal.[15,38,39] The values of q_m and K_L can be obtained from the slope of C_e/q_e *vs.* C_e and the intercept respectively.

The Freundlich isotherm (eqn (6)), denotes adsorption taking place onto a heterogenous (multiple layers) surface where the active sites are assumed to have different energies.[42,43]

$$q_e = K_f C_e^{\frac{1}{n}} \quad (6)$$

K_f $((\text{mg g}^{-1})\ \text{mol}^{-1}\ \text{L}^{-1})^{1/n})$ is the Freundlich isotherm constant, and n refers to the adsorption intensity of the Freundlich model. The values of K_f and n can be obtained from the slope of $\ln q_e$ *vs.* $\ln C_e$ and, the intercept respectively.[36,37] The n factor can also be used to indicate whether the adsorption process is chemical ($n > 1$) or physical ($n < 1$).[36,37]

The Dubinin–Radushkevich (D–R) (eqn (7)) isotherm describes the adsorption of metals onto a heterogenous adsorbent surface with Gaussian energy distribution.[36]

$$\ln q_e = \ln X_m - K_{ad}\varepsilon^2 \quad (7)$$

K_{ad} $(\text{mol}^2\ (\text{kJ}^2)^{-1})$ is the D–R isotherm constant that can be obtained from the plot of $\ln q_e$ *vs.* ε^2. X_m (mg g^{-1}) is the D–R theoretical saturation capacity (maximum adsorption capacity) that can be determined from the slope-intercept. ε is the Polanyi constant, expressed as eqn (8):

$$\varepsilon = RT \ln\left(1 + \frac{1}{C_e}\right) \quad (8)$$

R $(8.314\ \text{J (mol K)}^{-1})$ is the universal gas constant and T (K) is the absolute temperature.

The D–R isotherm constant can also be used to estimate the mean free energy (E_s (kJ mol^{-1})) (eqn (9)), which can be used to validate whether adsorption takes place *via* physical adsorption ($1 < E_s < 8$), ion-exchange ($8 < E_s < 16$), or chemical adsorption ($E_s > 20$).[8,13,37]

$$E_s = \frac{1}{\sqrt{2K_{ad}}} \quad (9)$$

The data presented in Table 3 indicated that the adsorption process conformed to the Langmuir isotherm model, as the correlation coefficients (R^2) of were closest to 1.[13,14] This suggests that Pt and Pd adsorbed onto both adsorbents in a monolayer fashion.[39]

The K_L values revealed that both adsorbents had a higher selectivity for Pd, which explains its higher recovery relative to Pt. For Pt, the K_L value was highest for TESP-BT-SG, suggesting a stronger affinity for this metal compared to APTES-SG, which aligns with the experimentally obtained data.[15,38,39]

From the Freundlich and D–R isotherms, the values of n and E_s were found to be greater than 1 and 20 respectively, suggesting that chemical adsorption of Pt and Pd onto both adsorbents.[13,37] These isotherm trends were consistent with data from our previous study, indicating similar equilibrium adsorption behaviour of the metals on the adsorbents.

The maximum experimental adsorption capacities (q_m), indicating the adsorbents' efficiency for metal recovery, are also listed in Table 3. In comparison to other adsorbents in the literature (Table S4†), the loading capacities of Pt and Pd on both adsorbents were moderate. Additionally, q_m values were combined with ligand concentrations to calculate the adsorbent-to-metal ratios. Table S3† shows that these ratios were smaller for TESP-BT-SG (Pt: 3.72; Pd: 2.05) than for APTES-SG (Pt: 19.06; Pd: 7.96), suggesting that a smaller amount of TESP-BT-SG would be needed to remove Pt and Pd from solution.[38,42] Furthermore, these ratios were lower than those reported in our previous study, especially for APTES-SG, highlighting its higher efficiency over the previous amine-based adsorbent (BTMSPA-SG).

3.4.1. Effect of contact time. The effect of contact time (0–1430 min) (Fig. 6b) was studied, showing rapid adsorption of Pt and Pd by both adsorbents within the first 90 minutes due to the high number of vacant sites at the start of the adsorption process.[13,14,37] After some time, as more metals occupy the active sites, the adsorption rate gradually decreases, reaching equilibrium.[14,39] The equilibrium phase for Pd adsorption was reached quickly, within 3 hours, by both TESP-BT-SG and APTES-SG, indicating fast and favourable adsorption. The highest Pt removal efficiency was observed after 6 hours for TESP-BT-SG and 24 hours for APTES-SG.

While both adsorbents showed similar behaviour in Pd recovery, TESP-BT-SG outperformed APTES-SG in Pt adsorption, making it a more efficient adsorbent as it effectively recovered both metals in a shorter time.

Table 3 Adsorption isotherm model parameters of Pt and Pd

		TESP-BT-SG		APTES-SG	
Isotherm models	Parameters	Pt	Pd	Pt	Pd
Langmuir	q_m (mg g^{-1})	29.01	28.66	25.06	32.73
	K_L (L mol^{-1})	2.13	71.18	0.61	73.00
	R^2	0.99	0.99	0.98	0.99
Freundlich	n	4.44	6.85	2.63	4.127
	K_F $((\text{mg g}^{-1})\ (\text{mol}^{-1}\ \text{L}^{-1})^{1/n})$	15.10	21.81	8.59	20.97
	R^2	0.60	0.37	0.50	0.73
(D–R)	E_s (kJ mol^{-1})	4450.96	9983.60	1196.33	6094.52
	X_m (mg g^{-1})	27.39	27.42	30.60	30.91
	R^2	0.86	0.30	0.86	0.95

3.5 Adsorption kinetics

The mechanism by which adsorption of Pt and Pd occurred onto the adsorbents was determined by correlating the contact time experimental data with the pseudo-first and second-order kinetic order models.[14,39] The rate of adsorption which is also known to be a good indicator for evaluating an adsorbent's performance was also determined from the kinetic model data.[14,39] The pseudo-first-order model (eqn (10)) describes adsorption that takes place through physisorption.[39] The pseudo-second-order model (eqn (11)) is indicative of chemical adsorption which involves covalency forces through the sharing of electrons between the metals and adsorbents.[39]

$$\log(q_e - q_t) = \log q_e - \frac{k_1 t}{2.303} \quad (10)$$

$$\frac{t}{q_t} = \frac{1}{k_2 q_e^2} + \frac{1}{q_e} t \quad (11)$$

q_t (mg g^{-1}) is the amount of metal adsorbed at time t. k_1 (min^{-1}) and k_2 (g mg^{-1} min^{-1}) are the rate constants of the pseudo-first and pseudo-second-order models, respectively.[43,44]

The obtained data in Table 4, indicated that the pseudo-second-order model best described the experimental data as the R^2 values were closer to 1 and the $q_{e(calc)}$ values were also consistent with the $q_{e(exp)}$ of this model.[13,14]

These results, therefore, suggest that chemical adsorption had taken place through a chemical reaction between the functional groups of the adsorbents and the Pt and Pd anionic metal complexes.[15,38,39] The rate of adsorption (k_2) was also higher for the pseudo-second-order model, thus further validating that the experimental data conformed to this model. Additionally, Pd exhibited higher k_2 values than Pt for both TESP-BT-SG and APTES-SG, thus confirming its fast kinetics of adsorption.[38]

3.5.1. Effect of competing ions. In PGM mining, Pt and Pd are often processed alongside metals like Mg, K, Ca, Fe, Co, Ni, and Zn, which co-occur in host ores and are released together in industrial waste solutions.[6,36,37] Thus, evaluating the selectivity of adsorbents for Pt and Pd in the presence of these competing ions is crucial. Competing ion concentrations were varied from 5–100 mg L^{-1}, while Pt and Pd were held at 5 mg L^{-1}, reflecting refinery conditions where competing ions are at elevated levels while PGMs remain relatively low.[6,36]

Results in Fig. 7 show that competing ions did not affect Pt and Pd adsorption, with both metals being significantly recovered. Low recovery of competing ions at pH 2 likely arises from their prevalent cationic forms, while Pt and Pd exist as anionic complexes ($[PtCl_6]^{2-}$ and $[PdCl_4]^{2-}$).[44–47] The protonated adsorbent surface repels cations but attracts anionic Pt and Pd, facilitating selective adsorption.[43–47] Koch *et al.* also found acylthioureas exhibit high selectivity for PGMs in highly acidic solutions.[48] Similarly, Kramer *et al.* reported that amine ligands form stable complexes with PGMs in acidic environments, while other metals do not exhibit this tendency.[11]

Pd recovery exceeded 98% for both adsorbents at all ion concentrations. Pt removal efficiency with TESP-BT-SG dropped from 97% to 87% (5–100 mg L^{-1}), with an even greater decrease observed with APTES-SG (97% to 54%).

Chassary *et al.*, attributed the preferential Pd recovery to differences in the chemistries of Pt and Pd, specifically in their chloro-complex formation and hydrolysis behaviours.[42] Pt(IV), more susceptible to hydrolysis, shows altered species distribution when Pd(II) is present, as Pd complexes diminish chloride ions needed to form Pt chloro-anions, thereby reducing Pt adsorption.[43,44]

TESP-BT-SG showed comparable selectivity to the previous acylthiourea adsorbent (DTMSP-BT-SG) for both metals, though with a lower ligand loading of 0.553 mmol g^{-1}, compared to 1.03 mmol g^{-1} for DTMSP-BT-SG. This lower loading yielded a higher ligand-to-metal adsorption ratio of 3.72 (Pt) and 2.05 (Pd) *versus* 4.15 (Pt) and 3.69 (Pd) for DTMSP-BT-SG (Table S3†). The reduced loading likely results from intramolecular hydrogen bonding, typical for mono-alkyl acylthioureas, which results in a bulkier conformation.[48] This is consistent with sharper C=O and C=S peaks in the ^{13}C CP MAS NMR spectrum of TESP-BT-SG and a shifted IR carbonyl stretch (1671 cm^{-1} for TESP-BT-SG *versus* 1685 cm^{-1} for DTMSP-BT-SG). This conformation would be significantly bulkier and loading density is expected to be lower (Fig S13†).[48]

APTES-SG showed improved selectivity for Pt and Pd (>97%) compared to the previous amine adsorbent, BTMSPA-SG (Pt < 50% and Pd 82%), likely due to APTES-SG's higher adsorption capacity. These results underscore the strong selectivity of both adsorbents for Pt and Pd, especially under the conditions tested (pH 2, dosage 0.5 g L^{-1}).

3.5.2. Comparing the adsorption efficiencies of the amines. Overall, the silica-anchored acylthioureas demonstrated superior adsorption efficiency compared to the silica-anchored amines, with the adsorption order for both Pt and Pd as follows: DTMSP-BT-SG ≈ TESP-BT-SG > APTES-SG >

Table 4 Kinetic model parameters of the Pt and Pd adsorption

		TESP-BT-SG		APTES-SG	
Kinetic models	Parameters	Pt	Pd	Pt	Pd
Pseudo-first-order	$q_{e(exp)}$ (mg g^{-1})	9.89	9.99	9.42	9.91
	$q_{e(cal)}$ (mg g^{-1})	2.55	2.13×10^{-4}	0.60	0.12
	k_1 (min^{-1})	-4.63×10^{-5}	-5.00×10^{-7}	-8.25×10^{-6}	-2.17×10^{-5}
	R^2	0.90	0.034	0.67	0.36
Pseudo-second-order	$q_{e(cal)}$ (mg g^{-1})	10.00	9.99	9.68	9.93
	k_2 (mg g^{-1} min^{-1})	0.0216	52.1365	0.0420	0.1992
	R^2	0.99	1.00	0.99	0.99

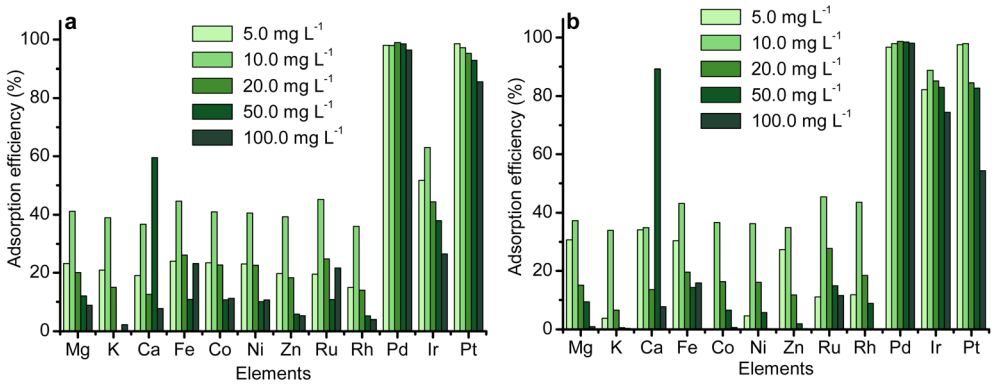

Fig. 7 Effect of competing ions on the recovery of Pt and Pd by (a) TESP-BT-SG and (b) APTES-SG (mass = 10 mg, pH = 2, conc. = 5 mg L^{-1}, temp. = 25 °C, time = 4 h, vol. = 20 mL, n = 2, RSD < 4%).

BTMSPA-SG. Ciesynska *et al.*, suggested that the metal extraction capabilities of amines depend on their structure and the type of substituents.[49,50] According to their findings, the extraction ability of amines for metal halides or nitrates generally increases in this order: primary < secondary < tertiary < quaternary, and also improves with a greater number of amine groups.[11,49–51] Contrary to this trend, our study found that the primary amine (APTES-SG) outperformed the secondary amine (BTMSPA-SG) under optimal conditions.[17]

As the pK_b values for both adsorbents were similar, additional factors such as surface area, steric effects, and rate constants were examined. Jal *et al.* noted that bulkier ligand groups reduce pore volume on solid supports (such as silica gel) by occupying more space, which in turn decreases surface area and limits the availability of active sites.[52] This effect is less evident with smaller molecules, which can provide more active sites by covering a larger surface area.[52,53] Our BET results supported this, showing that BTMSPA-SG had a lower surface area (130.06 m^2 g^{-1}) than APTES-SG (180.19 m^2 g^{-1}).[17]

The conformation of amine groups may also influence adsorption kinetics. When the primary amine (APTES) is anchored to the silica surface, it retains flexibility, whereas the secondary amine (BTMSPA) adopts a more rigid structure.[52] This flexibility may enhance APTES's activity and hinder BTMSPA's, a trend that aligned with our kinetic data.[54]

Moreover, we achieved a significantly higher amine loading on APTES-SG (2.45 mmol g^{-1}) compared to the 1.15 mmol g^{-1} reported by Kramer and colleagues, as well as to BTMSPA-SG (1.68 mmol g^{-1}), indicating that surface area and nitrogen content were critical factors in determining adsorption capacity.[11,12,17,52,53] The high amine loading may enable multiple protonated amines to interact with an anionic species, which would make adsorption even more favourable due to entropy considerations.

4. Conclusion

This study successfully synthesised the novel TESP-BT ligand and immobilised both TESP-BT and APTES onto silica gel. Structural analyses through NMR, FT-IR, SEM, TGA/DTA, PXRD, and XRF confirmed the structures of the ligand and adsorbents. Under optimal recovery conditions (pH 2, metal concentration of 5 mg L^{-1}, dosage of 0.5 g L^{-1} for Pd and 2.5 g L^{-1} for Pt), TESP-BT-SG efficiently recovered over 97% of both Pt and Pd. At these conditions, APTES-SG exhibited higher recovery for Pd (>97%) than for Pt (>83%). In solutions with increasing concentrations of competing ions (5–100 mg L^{-1}), both adsorbents showed strong selectivity for Pd (>98%), while Pt recovery declined with rising ion concentration, from 97–87% for TESP-BT-SG and 97–54% for APTES-SG. These results highlight TESP-BT-SG's superior adsorption efficiency for both metals over APTES-SG, which showed a stronger recovery for Pd over Pt.

Compared to our previous findings, the adsorption efficiency order was: DTMSP-BT-SG ≈ TESP-BT-SG > APTES-SG > BTMSPA-SG, with both acylthioureas displaying comparable performance. Among the amines, APTES-SG outperformed BTMSPA-SG. This difference in adsorption capacity was attributed to their exposed surface areas and ligand loading on the silica support. APTES-SG achieved a significantly higher ligand concentration (2.45 mmol g^{-1}) compared to BTMSPA-SG (1.68 mmol g^{-1}) and more than double the previously reported concentration (1.15 mmol g^{-1}), thereby providing more active sites for Pt and Pd capture.

In conclusion, the silica-anchored acylthioureas demonstrated excellent adsorption efficiency and selectivity for both Pt and Pd under the tested conditions, achieving equilibrium adsorption faster than the silica-anchored amines. This positions silica-anchored acylthioureas as promising and cost-effective extracting agents for Pt and Pd recovery from secondary sources, while the new, highly modified APTES-SG shows potential as a viable, cost-effective alternative with additional capacity for Ir extraction from solution.

To further improve on this work, the selectivity of the adsorbents can be evaluated in competing ions solutions containing noble metals such as Ag and Au, to provide deeper insights into their preferential adsorption behaviour toward Pt and Pd. Additionally, investigating the adsorption performance of different oxidation states of Pt (II *vs.* IV) and Pd (II *vs.* IV) is recommended to better understand the impact of speciation on adsorption efficiency and mechanism.

Data availability

The data supporting the findings of this study are available within the article and the ESI.†

Conflicts of interest

There are no conflicts to declare.

Acknowledgements

The authors thank the National Research Foundation (NRF (149354)) for financial support and the University of the Witwatersrand for the research facilities.

References

1 O. Grad, M. Ciopec, A. Negrea, N. Duțeanu, G. Vlase, P. Negrea, C. Dumitrescu, T. Vlase and R. Vodă, *Sci. Rep.*, 2021, **11**, 2016.
2 I. Chidunchi, M. Kulikov, R. Safarov and E. Kopishev, *Heliyon*, 2024, **10**, e25283.
3 L. Chen, K. Wu, M. Zhang, N. Liu, C. Li, J. Qin, Q. Zhao and Z. Ye, *Chem. Eng. J.*, 2023, **466**, 43082.
4 D. Zhang, L. MacDonald, P. Raj and A. Karamalidis, *Chem. Eng. J.*, 2024, **494**, 152948.
5 L. MacDonald, D. Zhang and A. Karamalidis, *Resour. Conserv. Recycl.*, 2024, **205**, 107590.
6 M. R. Awual, M. A. Khaleque, Y. Ratna and H. Znad, *J. Ind. Eng. Chem.*, 2015, **21**, 405–413.
7 K. Liu and X. Gao, *Environ. Pollut.*, 2019, **255**, 113192.
8 M. R. Awual, M. M. Hasan, M. Naushad, H. Shiwaku and T. Yaita, *Sens. Actuators, B*, 2015, **209**, 790–797.
9 J. Lee, H. Hong, K. Chung and S. Kim, *Sep. Purif. Technol.*, 2020, **246**, 116896.
10 S. Swaminathan, P. Jerome, R. Deepak, R. Karvembu and T. Oh, *Coord. Chem. Rev.*, 2024, **503**, 215620.
11 J. Kramer, W. L. Driessen, K. R. Koch and J. Reedijk, *Hydrometallurgy*, 2002, **64**, 59–68.
12 J. Kramer, N. E. Dhladhla and K. R. Koch, *Sep. Purif. Technol.*, 2006, **49**, 181–185.
13 M. Li, S. Tang, Z. Zhao, X. Meng, F. Gao, S. Jiang, Y. Chen, J. Feng and C. Feng, *Chem. Eng. J.*, 2020, **386**, 123947.
14 A. Mavhungu, R. K. Mbaya and M. L. Moropeng, *Int. J. Chem. Eng. Appl.*, 2013, **4**, 354–358.
15 A. N. Nikoloski, K. L. Ang and D. Li, *Hydrometallurgy*, 2015, **152**, 20–32.
16 R. G. Pearson, *J. Am. Chem. Soc.*, 1963, **85**, 3533–3539.
17 M. R. Mphahlele, A. K. Mosai, H. Tutu and I. A. Kotzé, *RSC Adv.*, 2024, **14**, 7507–7516.
18 A. Erdem, T. Shahwan, A. Ağır and A. E. Eroğlu, *Chem. Eng. J.*, 2011, **174**, 76–85.
19 A. Purwanto, Y. Yusmaniar, F. Ferdiani and R. Damayanti, *AIP Conf. Proc.*, 2017, **1891**, 030018.
20 J. Reijenga, A. Van Hoof, A. Van Loon and B. Teunissen, *Anal. Chem. Insights*, 2013, **8**, DOI: 10.4137/ACI.S12304.
21 H. N. Po and N. M. Senozan, *J. Chem. Educ.*, 2001, **78**, 1499.
22 G. Khaira and A. Kot, *Chemistry LibreTexts*, https://chem.libretexts.org/Bookshelves/Physical_and_Theoretical_Chemistry_Textbook_Maps/Supplemental_Modules_(Physical_and_Theoretical_Chemistry)/Acids_and_Bases/Buffers/Henderson-Hasselbalch_Approximation, accessed May 5, 2024.
23 P. Thaplyal and P. C. Bevilacqua, *Methods Enzymol.*, 2014, **549**, 189–219.
24 L. Zaharani and N. G. Khaligh, *Chem. Teach. Int.*, 2023, **5**, 427–437.
25 H. Sohn and J. Thornton, *Chemistry LibreTexts*, https://chem.libretexts.org/Ancillary_Materials/Demos_Techniques_and_Experiments/General_Lab_Techniques/Titration/Titration_of_a_Weak_Acid_with_a_Strong_Base accessed May 5, 2024.
26 K. Cox and C. Chang, *Chemistry LibreTexts*, https://chem.libretexts.org/Ancillary_Materials/Demos_Techniques_and_Experiments/General_Lab_Techniques/Titration/Titration_of_a_Weak_Base_with_a_Strong_Acid, accessed May 6, 2024.
27 A. Saeed, U. Flörke and M. F. Erben, *J. Sulfur Chem.*, 2013, **35**, 318–355.
28 A. N. Mautjana, J. D. Miller, A. Gie, S. A. Bourne and K. R. Koch, *Dalton Trans.*, 2003, **10**, 1952–1960.
29 G. Perez, E. Erkizia, J. J. Gaitero, I. Kaltzakorta, I. Jiménez and A. Guerrero, *Mater. Chem. Phys.*, 2015, **165**, 39–48.
30 P. E. Imoisili, E. C. Nwanna and T.-C. Jen, *Processes*, 2022, **10**, 2440.
31 Z. A. Alothman and A. W. Apblett, *J. Hazard. Mater.*, 2010, **182**, 581–590.
32 R. K. Sharma, M. Mishra, S. Sharma and S. Dutta, *J. Coord. Chem.*, 2016, **69**, 1152–1165.
33 V. Zeleňák, M. Skříňská, A. Zukal and J. Čejka, *Chem. Eng. J.*, 2018, **348**, 327–337.
34 S. Silviana, A. A. Janitra, A. N. Sa'adah and F. Dalanta, *Ind. Eng. Chem. Res.*, 2022, **61**, 9283–9299.
35 S. Jodeh, G. Hanbali, I. Warad, H. Lgaz, D. Jodeh, S. Radi and S. Tighadouini, *Appl. J. Environ. Eng. Sci.*, 2015, **1**, 66–84.
36 A. K. Mosai, L. Chimuka, E. M. Cukrowska, I. A. Kotzé and H. Tutu, *Chemosphere*, 2020, **239**, 124768.
37 A. K. Mosai, L. Chimuka, E. M. Cukrowska, I. A. Kotzé and H. Tutu, *Environ. Dev. Sustain.*, 2020, **23**, 7041–7062.
38 A. N. Nikoloski and K. L. Ang, *Miner. Process. Extr. Metall. Rev.*, 2013, **35**, 369–389.
39 A. K. Mosai, *Miner. Eng.*, 2021, **163**, 106770.
40 W. I. Congdon and J. T. Edward, *J. Am. Chem. Soc.*, 1972, **94**, 6099–6104.
41 K. Khunathai, K. Inoue, K. Ohto, H. Kawakita, M. Kurata, K. Atsumi, H. Fukuda and S. Alam, *Solvent Extr. Ion Exch.*, 2013, **31**, 320–334.
42 P. Chassary, T. Vincent, J. Sanchez Marcano, L. E. Macaskie and E. Guibal, *Hydrometallurgy*, 2005, **76**, 131–147.
43 T. G. Asere, S. Mincke, K. Folens, F. Vanden Bussche, L. Lapeire, K. Verbeken, P. Van Der Voort, D. A. Tessema,

G. Du Laing and C. V. Stevens, *React. Funct. Polym.*, 2019, **141**, 145–154.
44 H. Sharififard, M. Soleimani and F. Z. Ashtiani, *J. Taiwan Inst. Chem. Eng.*, 2012, **43**, 696–703.
45 Z. Hubicki and A. Wołowicz, *J. Hazard. Mater.*, 2009, **164**, 1414–1419.
46 S. Lin, W. Wei, X. Wu, T. Zhou, J. Mao and Y. S. Yun, *J. Hazard. Mater.*, 2015, **299**, 10–17.
47 W. Wang, X. Liu, X. Wang, L. Zong, Y. Kang and A. Wang, *Front. Chem.*, 2021, **9**, 662482.
48 K. R. Koch, *Coord. Chem. Rev.*, 2001, **216–217**, 473–488.
49 A. Cieszynska and D. Wieczorek, *Hydrometallurgy*, 2018, **175**, 359–366.
50 T. H. Nguyen, C. H. Sonu and M. S. Lee, *J. Ind. Eng. Chem.*, 2015, **32**, 238–245.
51 B. Swain, C. Mishra and K. K. Sahu, *Hydrometallurgy*, 2010, **104**, 1–7.
52 P. Jal, S. Patel and B. K. Mishra, *Talanta*, 2004, **62**, 1005–1028.
53 O. E. Fayemi, J. A. Adekoya, E. E. Ebenso and A. S. Adekunle, *Sep. Sci. Technol.*, 2014, **50**, 1497–1506.
54 C. Huang, J. Tian, J. Yan, M. Li and X. Li, *Materials*, 2020, **13**, 2958.